Combust. Sci. and Tech., 2001, Vol. 164, pp. 209-237
Reprints available directly from the publisher
Photocopying permitted by license only

Combustion of Aluminum Particles in Carbon Dioxide

SERGIO ROSSI[a], EDWARD L. DREIZIN[b*] and CHUNG K. LAW[c]

[a]Politecnico di Torino, Torino, Italy, [b]New Jersey Institute of Technology, Newark, NJ 07102 and [c]Princeton University, Princeton, NJ

(Received May 5, 2000; In final form November 30, 2000)

Recently, it has been determined that Martian soil is rich in metallic elements such as Al, Mg, Si, and Fe. Because Martian atmosphere consists largely of CO_2, a propulsion system using metals as fuel and CO_2 as oxidizer would enable one to utilize Mars's resources very efficiently. Currently, experimental data on metal combustion in CO_2 are scarce and an experimental study of aluminum particle combustion in CO_2 is presented in this work. Uniform initial size and temperature metal particles are produced and ignited using a pulsed microarc. The free-falling particles burn in the atmospheric pressure CO_2. Flame radiation is monitored in real time, the temperature is measured using a three-color optical pyrometer coupled to a computer-based data acquisition system. Particles are quenched at different burn times and their surface morphology and internal compositions are studied using electron microscopy techniques. Preliminary experiments with particles of commercially available aluminum-rich Al-Mg and Al-Si alloys are also performed. The size of the burning particles was observed to decrease and more than 94 % of aluminum was consumed by combustion in CO_2. It was found that the rate of aluminum combustion in CO_2 is faster than that in air and the dependence of particle burn time from particle size is best described by $t \sim d^{2.5}$ rather than by $t \sim d^2$-law. Flame radiation measurements showed that the vapor-phase reaction is significant only during the initial period of combustion. The measured temperature was steady and around 3000 °C during most of the combustion time. The estimated adiabatic flame temperature is reasonably close to the experimental value. Particles quenched on Si wafers were surrounded by spherical smoke clouds and the particle surfaces were coated with a layer of partially coalesced oxide nano-spheres. Surfaces of the completely burnt particles did not have a continuous oxide coating, instead, a number of oxide spheres in the size range of 1 – 5 μm were attached to the particle surface. Interiors of the particles rapidly quenched on aluminum foil were uniform and contained significant amounts of carbon and oxygen. Some increase in the overall carbon and oxygen content was observed at longer combustion times. Interiors of the completely burnt particles contained several mixed phases, including layers of two non-stoichiometric aluminum oxycarbides and pure aluminum inclusions. None of the oxycarbide phases detected in the quenched or burnt particles was similar to the aluminum oxycarbides described in literature. Analyses of the experimental results have indicated possible importance of the thermophoretic flows in the transport of the vapor-phase reaction products. It has also been suggested that the internal phase changes affect significantly the temperature and rate of aluminum combustion in CO_2.

* Corresponding Author: Phone: (973) 596–5751, Fax: (973) 642–4282, E-Mail: dreizin@njit.edu

I. INTRODUCTION

Recent studies have determined that Martian soil is rich in metallic elements such as Al, Mg, Si, and Fe (Rieder, et al., 1997). It is also well known that Martian atmosphere consists largely of CO_2 and thus a propulsion system using metals as fuel and CO_2 as oxidizer would enable one to utilize Mars's resources very efficiently. Metals are known to have very high oxidation enthalpies and thermo-chemical estimates predict that many of the metals will burn efficiently in CO_2. For example, adiabatic flame temperatures at a constant (atmospheric) pressure computed using an AFAL specific impulse code (Selph and Hall, 1991) and initial temperature of 300 K are presented in Table I for several stoichiometric metal-CO_2 flames.

TABLE I Estimated adiabatic flame temperatures of several metals in CO_2

Metallic element	*Adiabatic Flame Temperature, K*
Titanium	3550
Aluminum	3090
Magnesium	2995
Silicon	2230
Boron	1960

Currently, experimental data for metal combustion in CO_2 are sparse. A series of experiments have been conducted in Russia addressing combustion of magnesium in CO_2 (Shafirovich and Goldshleger, 1992; Shafirovich and Goldshleger, 1997, Valov, et al., 1994). Magnesium particles could be ignited and burnt, and their combustion times and temperatures were measured. The particles burning temperatures were found to be fairly high, however, ignition difficulties were reported. Experiments with Al, Mg, and a Mg-Al alloy have been also reported in which laser was used to ignite the levitating particles (Marion et al., 1996; Marion et al., 1997; Legrand, et al., 1998; Legrand et al., 1999). However, ignition difficulties were observed in that work and interfered with the comparison of the combustion behavior of pure metals and alloys. Laser ignited aluminum particle combustion in CO_2 has been also recently studied by Bucher et al., 1999, who have suggested that the aluminum flame structure in pure CO_2 is that of the classical diffusion flame. However, flame images for both Mg and Al particles burning in CO_2 presented by Legrand et al., 1999, showed significant differences between the flame structures for these two metals, e.g., for aluminum particle, metal surface appeared much brighter than the stand-off radiation zone whereas for magnesium, particle surface was invisible on the background of the stand-off

radiation. These differences were interpreted as indicating the importance of the exothermic surface reactions for aluminum (Legrand et al., 1999).

Recent experimental research on combustion of different metal particles in air and other oxygen/inert gas mixtures (Dreizin, et al., 1993, Dreizin 1996; Molodetsky, et al., 1997; Molodetsky, et al., 1998; Dreizin 1999a; Dreizin 1999b) used free-falling uniform metal particles formed and ignited in a pulsed micro-arc (Suslov and Dreizin, 1993). Particles burned in a controlled atmosphere, and their temperatures were monitored using an optical pyrometer. Partially burned metal particles were rapidly quenched and their compositions and structures were analyzed. Burning particle temperature and radiation histories were thus correlated with the evolution of their internal compositions. This research for the first time conclusively showed that heterogeneous reactions and internal phase changes play important roles in the combustion of many metals, including aluminum and magnesium, usually considered burning in the vapor-phase. Since that experimental approach proved effective with a number of metals burning in air and other gas mixtures, it appeared useful to exploit it for characterization of metal combustion in carbon dioxide. The objective of this work was to characterize combustion of metals in CO_2 experimentally, investigate the combustion mechanisms and possible relationship between vapor-phase, surface, and internal reactions and the combustion scenario.

Aluminum is currently the only metal used in practical propellants due to its relatively low cost and high combustion enthalpy. Therefore, aluminum was selected for the first series of experiments on metal combustion in CO_2 using a pulsed microarc apparatus. In addition, preliminary results have been obtained for some commercially available aluminum-rich Al-Si and Al-Mg alloys.

II. EXPERIMENTAL

APPARATUS

The experimental apparatus is built around a micro-arc GEnerator of Monodispersed Metal Droplets (GEMMED) used in the previous metal particle combustion research (e.g., Dreizin 1996, Molodetsky, et al., 1997) ensuring repeatable formation and ignition of uniform metal droplets with controllable initial temperatures and velocities. The rapid melting of a consumable (metal) wire anode in a pulsed micro-arc discharge forms metal droplets. The electric discharge pulse continues until the droplet is at its maximum size determined by the balance of the surface tension force versus electron pressure and electrodynamic forces exerted on the droplet by the micro-arc. At the end of the micro-arc pulse, the

molten droplet breaks away from the wire anode, leaving at a reproducible velocity, size, and temperature. The initial temperatures for the droplets of most metals can be adjusted in the range from the metal melting to its boiling point, so that the molten droplets ignite immediately upon formation in an oxidizing environment. In this work, the micro-arc electrodes are housed in a rectangular 905 × 305 × 305 mm chamber. The chamber is built of 12.7 mm thick transparent Lexan® sheets around a frame made of 25 × 25 mm aluminum bars. It was leak tested in the pressure range of 0.5 to 1.3 atm. The chamber is equipped with 4 gas ports and several feedthroughs for electric power and electrode positioning. Before each experiment the chamber is flushed with a volume of pure CO_2 that is ten times the total volume of the chamber. The chamber then is filled with CO_2 to a pressure slightly greater than atmospheric (ca., by 5 kPa). That pressure is maintained during the experiments to prevent any leakage of ambient air. The purity of the gas environment is verified using gas chromatography. In addition to the pure aluminum wire anode, two Al-Mg and Al-Si alloy wires readily available commercially were used in a limited number of experiments. Wire materials used and respective particle sizes produced in these experiments are described in Table II.

TABLE II Materials used in experiments

Wire material	*Supplier*	*Particle sizes*
99.95 % pure Al	California Fine Wire Co.	108 – 250μm
Al – 5% Mg alloy	California Fine Wire Co.	200, 280 μm
Al – 1 % Si alloy	Goodfellow Co.	165 μm

OPTICAL DIAGNOSTICS

Streaks of burning particles are photographed using a 35 mm camera. A three-color pyrometer records burning particle radiation histories at three wavelengths. The pyrometer included a three-furcated fiber optics bundle that split the light between three channels. Each channel included an interference filter and a photo-multiplier. Two burning particle color temperatures are computed using the three-recorded radiation histories and the pyrometer calibration curve. The pyrometer was calibrated using a strip-lamp in the temperature range of 1600–2300°C. Because aluminum was primarily used in these experiments, the wavelengths of the pyrometer channels (410, 500 and 568 nm) were chosen to minimize the AlO bands radiation (Pearse and Gaydon, 1976). In separate experiments, two optical channels are used to compare the radiation of a vapor phase AlO band with the black body radiation. Using two interference filters

with very close wavelengths of 500 and 510 nm, the AlO band radiation (510 nm, see Pearse and Gaydon, 1976) is compared to the black body radiation (500 nm) recorded simultaneously.

SAMPLE MORPHOLOGY AND COMPOSITION ANALYSES

An adjustable height stand is positioned inside the chamber so that the free-falling burning particles can be quenched at different burn times. Particles are quenched using silicon wafers and, in different experiment, thin aluminum foils positioned at different heights inside the chamber. The particles that impinge onto the foil penetrate about halfway through and are welded into it; this quenching method provides a high cooling rate (up to 10^6 °C/s) and does not cause strong particle deformation. Particles quenched on the foil are recovered, embedded into epoxy and cross-sectioned. Both cross-sectioned and intact particles are studied using scanning electron microscopy techniques. Quenched particle surfaces and adjacent smoke cloud traces on silicon wafers are examined using a Philips XL30 field emission microscope, their elemental compositions were analyzed using a Princeton Gamma Tech Energy Dispersive Spectrometer (EDS). A six spectrometer CAMECA SX50 electron probe micro-analyzer equipped with a wavelength dispersive spectrometer (WDS) was used for more precise elemental composition measurements in particle cross-sections. Materials standards were prepared for the WDS calibration using SiC (calibration of carbon), Al_2O_3, (calibration of oxygen and aluminum) and pure aluminum. Standards as well as quenched particle samples were placed in a half-inch pellet of epoxy, cross-sectioned and polished. Because of the need to analyze carbon content in the samples, a 15Å thick coating layer of iridium was used instead of a more traditional carbon coating to cover each specimen in order to limit the charging of the samples by the electron beam. Since the intensity of the back-scattered x-rays depends on the distances between the electron beam source, sample, and detector, special care was taken in making the pellets containing all the specimens, including the standards, of the same height.

III. RESULTS

COMBUSTION TIMES

The measured combustion times are plotted in Fig. 1 against particle size for pure aluminum burned in CO_2. For reference, combustion times for the same ini-

tial size and temperature aluminum particles in air are also measured and shown in Fig. 1. The combustion times in air are in good agreement with the earlier reported data (Prentice, 1971; Wilson and Williams, 1971; Dreizin, 1996). Dashed lines shown in Fig. 1 represent the d^2-law fits with the lower and higher limits for the evaporation coefficient proposed by Wilson and Williams, 1971 to describe experimental data on aluminum particle combustion times reported in a number of earlier publications. In CO_2, shorter combustion times are consistently measured for all the particle sizes. Note also that the d^2-fit successfully applied for aluminum particle combustion times measured in air does not hold for the combustion times measured in CO_2. Instead, a fit using $t \sim d^{2.5}$ was found to adequately describe the experimental data.

Combustion times measured for alloy particles are compared against those for pure aluminum particles of the same size in Table III. The slightly shorter combustion times observed for alloys in a limited number of experiments that have been conducted indicate a faster burning rate and thus a possible advantage in using alloys versus pure metals. Additional experiments are needed to verify this suggestion.

TABLE III Comparison of combustion times for pure Aluminum and Alloy particles

Environment	*Material*	*Particle Size, μm*	*Combustion Time, ms*	*Experimental Error, %*
Air	Pure Aluminum	165–200	75–129	9.3–18.8
	Al-5% Mg	165	62	11.0
	Al-1% Si	200	118	18.8
CO_2	Pure Aluminum	165	45	11.2
	Al-5% Mg	165	47	9.4
	Al-1% Si	200	69	13.8

BURNING PARTICLE DIAMETER

In a series of experiments the diameters of quenched particles were measured at different quench times. The initial diameter used in these experiments was 250 ± 18 μm. During combustion, the particle diameter decreased. A plot showing the diameters of quenched particles versus the combustion time is shown in Fig. 2. The completely burnt particle diameter is also shown in Fig. 2, it was reduced to about 100 ± 5 μm, i.e., about 94 % of the initial particle volume was depleted. This can be compared to the droplet depletion in air as measured by Dreizin, 1996. The $d_{final}/d_{initial}$ is about 0.3 in air while in CO_2 it is about 0.4. One conclusion is that the particle is burnt nearly to completion in both cases. This con-

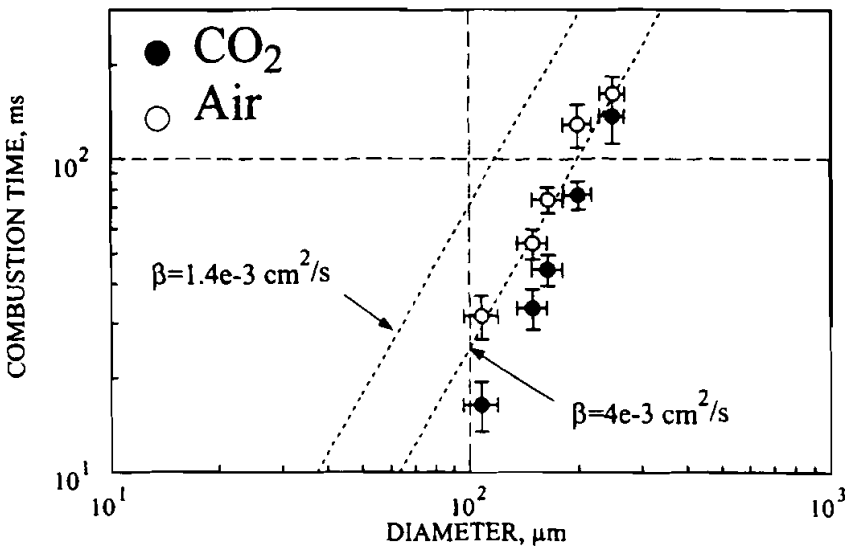

FIGURE 1 Combustion times of aluminum particles measured in air and CO_2. Dashed lines show extrapolation of experimental results for aluminum combustion in air by Wilson and Williams, 1971

clusion becomes even stronger considering that, as discussed below, the residual particles contained only minutes of pure aluminum.

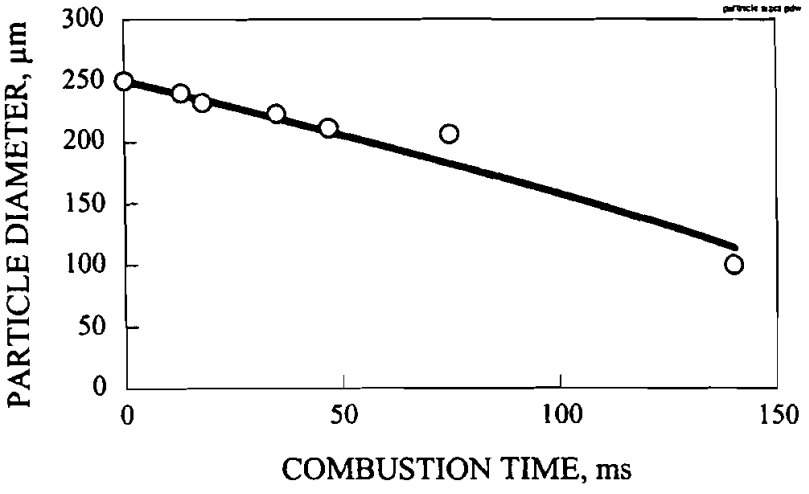

FIGURE 2 Temporal change in diameter of aluminum particles burning in CO_2. Initial particle diameter 250 μm

BURNING PARTICLE RADIATION

In order to distinguish between the radiation produced by the reacting vapor phase species and thermal black body radiation, interference filters were used. One of the bandpass filters was chosen with the central wavelength coinciding with the 510 nm band of the AlO radiation Pearse and Gaydon, 1976. The second filter had a central wavelength of 500 nm, where no AlO bands are reported. Both filters had 10 nm-wide half-bandwidth. The wavelengths selected by these filters were close, so that the direct comparison of the measured radiation intensities could be made to assess the intensity of the AlO radiation. A typical example of the two radiation intensity histories simultaneously measured at the mentioned above wavelengths for a 250 μm initial diameter aluminum particle burning in CO_2 is shown in Fig. 3. The AlO radiation is initially greater than that of black body, but after about one third of the combustion time the two signals become indistinguishable. This comparison of the two radiation signals indicates that the vapor-phase combustion is significant early after particle ignition, and becomes less significant at longer combustion times.

A similar comparison of the AlO versus black body radiation intensities was made for aluminum burning in air, as also illustrated in Fig. 3. During a brief initial period of combustion, the AlO radiation intensity increases and becomes greater than that of black body. It can be suggested that the vapor-phase flame was being established during this period. Afterwards, the AlO radiation remains significantly stronger than the black body radiation, indicating intensive vapor phase reaction for the most of the particle combustion time. During the third combustion stage (Dreizin, 1996), after about 65 % of the total combustion time, the intensities of both radiation signals become indistinguishable.

Streaks of the falling droplets were recorded using a 35 mm camera placed in front of the combustion chamber. An example of a characteristic particle streak is given in Fig. 4. The streak images exhibit a fairly stable radiation intensity. At the peak intensity level, small oscillations of the radiation intensity are noticeable. Considering an average speed of about 2 m/s and an average combustion time of 120 ms for a particle of 250 μm diameter, it is estimated that these oscillations occur at approximately 40 ms after particle ignition. An interesting feature observed clearly and consistently from the particle streaks is the presence of radiation jumps resembling "spear-points", previously observed for zirconium burning in pure oxygen (e.g., Nelson, 1967) and for several metals burning in air (Dreizin et al., 1993). These radiation jumps always occurred when the overall radiation intensity decreased significantly, and thus, they could not be clearly identified in the recorded radiation traces set up to capture the entire range of the radiation intensities.

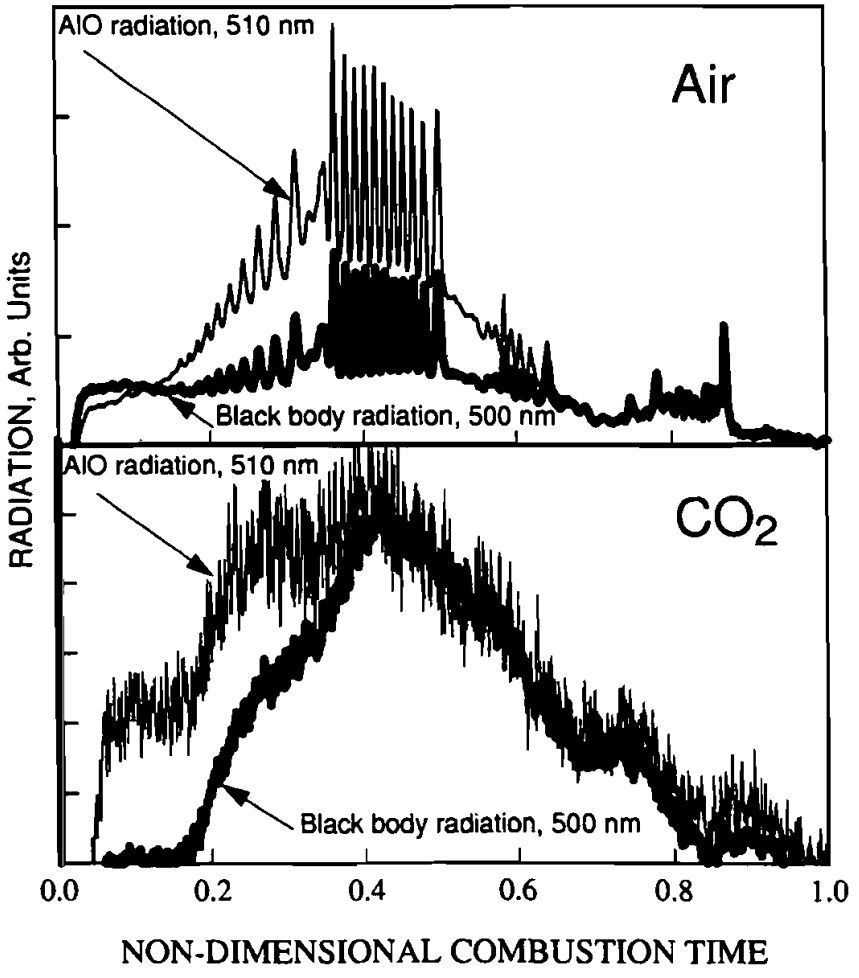

FIGURE 3 Radiation traces measured at 500 and 510 nm (for black body and AlO radiation, respectively) for aluminum particles burning in air and CO_2

TEMPERATURE MEASUREMENTS

The temperature measurements were compared for particles burned in CO_2 and in air. Typical examples of the measured temperature histories of particles burning in both environments are shown in Fig. 5. In both cases, a steady temperature plateau was observed. The particles burning in CO_2 show a shorter plateau than that for the same size aluminum particles burning in air. However, the ratio of the steady temperature plateau time duration over the entire combustion time was

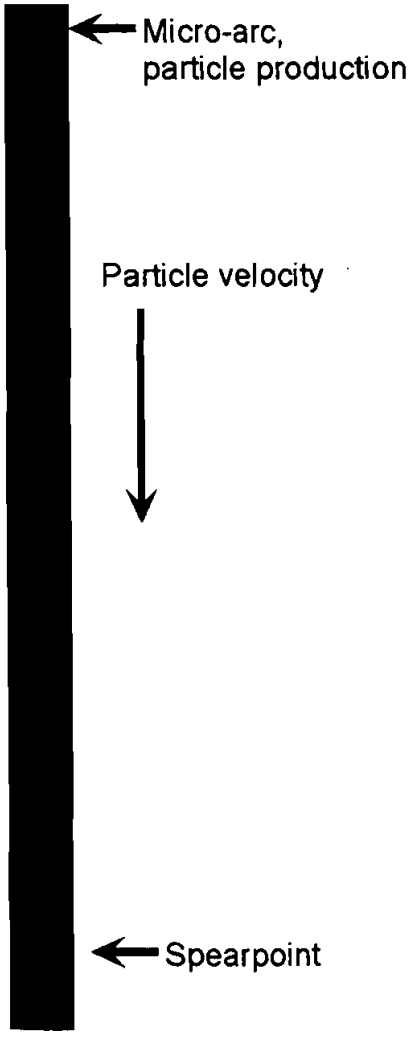

FIGURE 4 Streak of aluminum particle burning in CO_2

greater for CO_2 than for air. It is interesting to note that the maximum combustion temperatures measured in this work for aluminum particles burning in CO_2 (2930 ± 200 °C) are higher than those measured for aluminum particle burning in air (2730 ± 200 °C). The higher combustion temperatures in CO_2 were observed within the entire range of the examined particle diameters (from 165 to 250 μm). Since both the particle surface and the flame zone were in the field of view of the pyrometer, the measured temperatures was biased to the hottest regions in the

field of view and could be interpreted as the maximum temperatures in the flame zone.

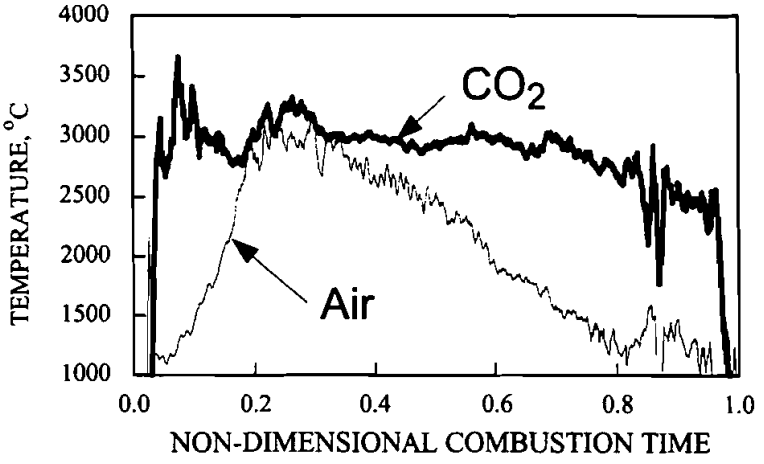

FIGURE 5 Typical examples of temperature histories of aluminum particles burning in CO_2 and air

SMOKE CLOUDS SURROUNDING QUENCHED PARTICLES

Particles of 250 μm initial diameter were quenched at combustion times ranging from 13 ms to 75 ms, the entire burn time for these particles was about 140 ms. All the quenched particles were surrounded by spherical smoke clouds, apparently the residue from the products of the vapor phase combustion. A typical example of a particle quenched on silicon wafer and surrounded by a smoke cloud is shown in Fig. 6. The smoke cloud formed a ring with the internal diameter of about 360 ± 15 μm and external diameter of about 1000 ± 100 μm at all the used quench times. Close-up images showed that the clouds consisted of spheres with diameters between 70 and 160 nm, as shown for example in Fig. 7.

To assess the elemental compositions of the smoke cloud's fine particles, three zones within the cloud were selected. Internal zone was defined within the 30 μm range from the particle surface, middle zone was defined at the central part of the cloud, i.e., at about 100 μm from the particle surface, and, finally, external zone was within the 30 μm range from the edge of the cloud. An EDS detector was employed for the elemental composition analyses. Quantitative results of the composition analyses are presented in Table IV. At both 13 and 42 ms quench times, measurable amounts of carbon were found in the internal part of the cloud. Only oxygen and aluminum were detected in the middle and external parts of the

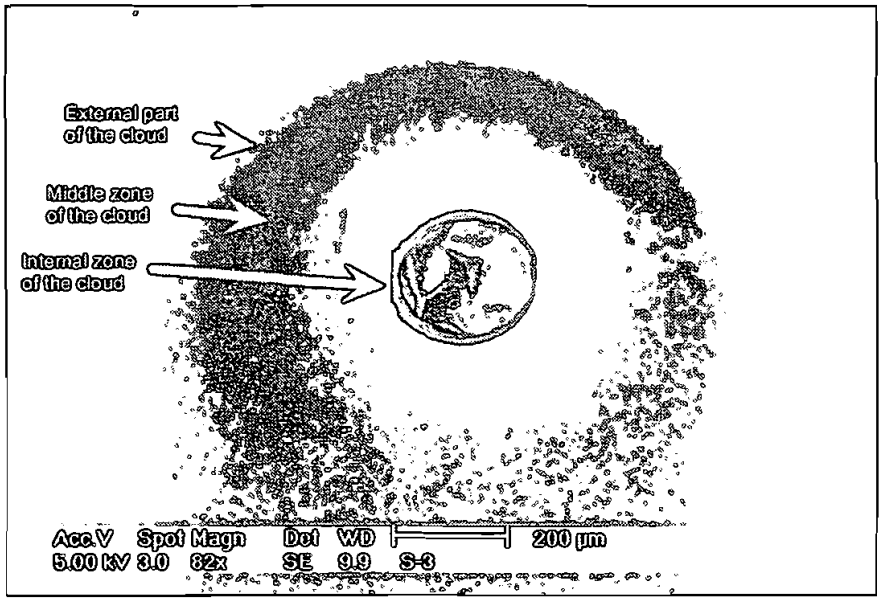

FIGURE 6 Aluminum particle quenched from CO_2 on silicon wafer

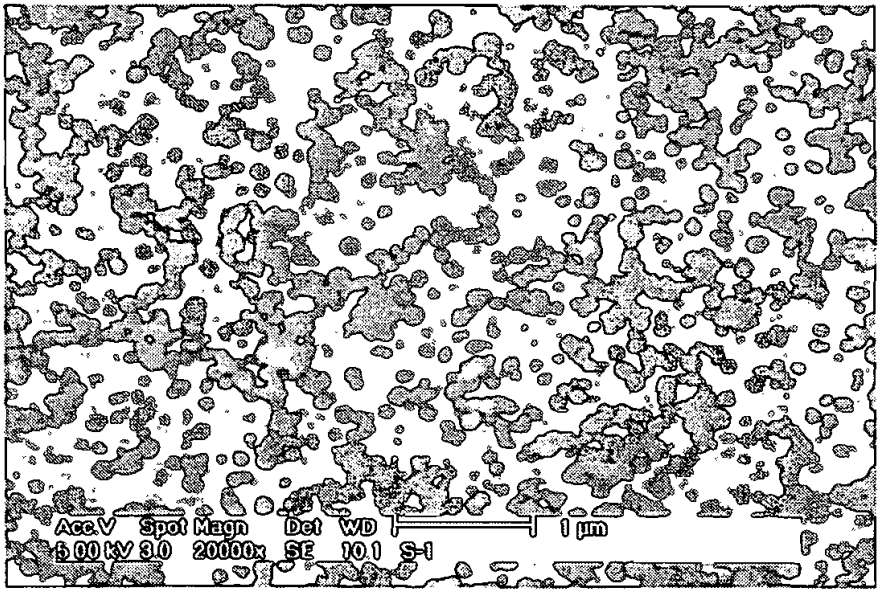

FIGURE 7 Close-up view of smoke cloud particles surrounding aluminum droplet quenched from CO_2 on silicon wafer

clouds at all combustion times, their concentrations were close to those in stoichiometric Al_2O_3. At a longer quench time (74 ms), carbon was not detected in any part of the cloud.

QUENCHED PARTICLE SURFACE

A typical SEM image of the surface of a particle burning in $CO_2$and quenched on silicon wafer is shown in Fig. 8. For most quenched particles, a layer composed of partially coalesced nano-particles, similar in morphology to those found in the cloud, was observed to cover the entire visible portion of the particle surface. The visible number density of the nano-particles covering the surface of the quenched particle (in the order of 60 μm^{-2}) was noticeably greater than the visible number density of similar nano-particles in the cloud immediately adjacent to the quenched particle surface (varied in the range of 30–40 μm^{-2}). Measured atomic concentrations of aluminum and oxygen in the particle surface layer were close to those in stoichiometric Al_2O_3. Interestingly, no carbon was detected in the layer of nano-particles covering the surface of the quenched aluminum droplet.

A region without oxide layer was observed on a surface of particle quenched at 42 ms, as shown in Fig. 9. Elemental analysis showed that the composition of the oxide-free particle surface included around 10 % of carbon, 50 % of oxygen, and 40 % of aluminum.

Samples of the completely burnt particles were also collected and studied using electron microscopy techniques. An image of a typical burnt particle is shown in Fig. 10. Oxide layers were not found on surfaces of these particles. Instead, the surface is covered with multiple cracks and, most remarkably, with multiple, approximately 1–5 μm diameter spheres. The bulk surface elemental composition was found to consist of approximately 10 % carbon and 90 % aluminum. The composition of the spheres was found to be that of stoichiometric Al_2O_3. Detailed examination of the close-up images of burnt particle surfaces, like that shown in Fig. 11, shows sets of smaller, submicron size spheres that appear to be growing from the cracks in particle surface; these smaller spheres could be precursors for the formation of the larger ones.

QUENCHED PARTICLE CROSS-SECTIONS AND INTERNAL COMPOSITIONS

Particles rapidly quenched by impinging on aluminum foil were cross-sectioned and their internal elemental compositions were analyzed. The surface oxide layer observed on quenched particles was not preserved during the cross sectioning so

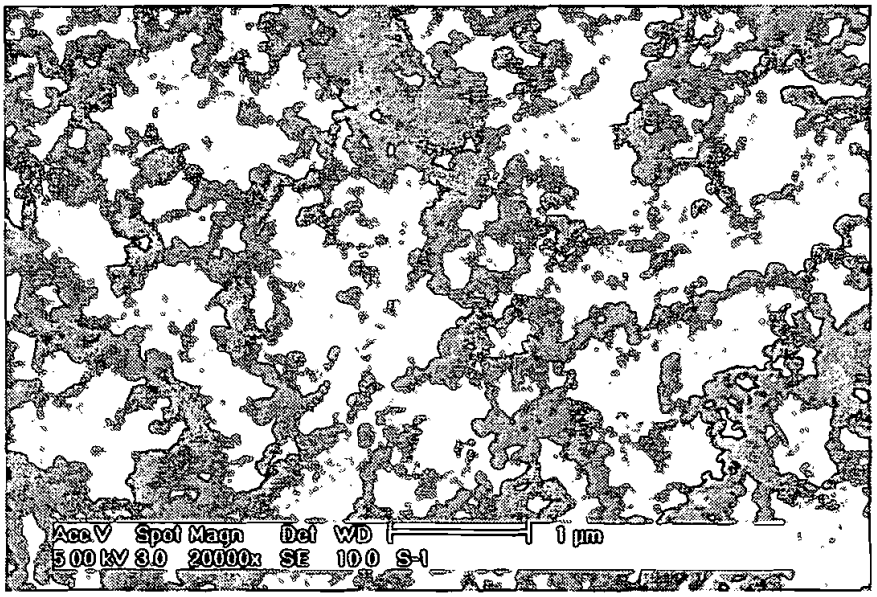

FIGURE 8 Close-up view of oxide particles coating aluminum droplet quenched from CO_2 on silicon wafer

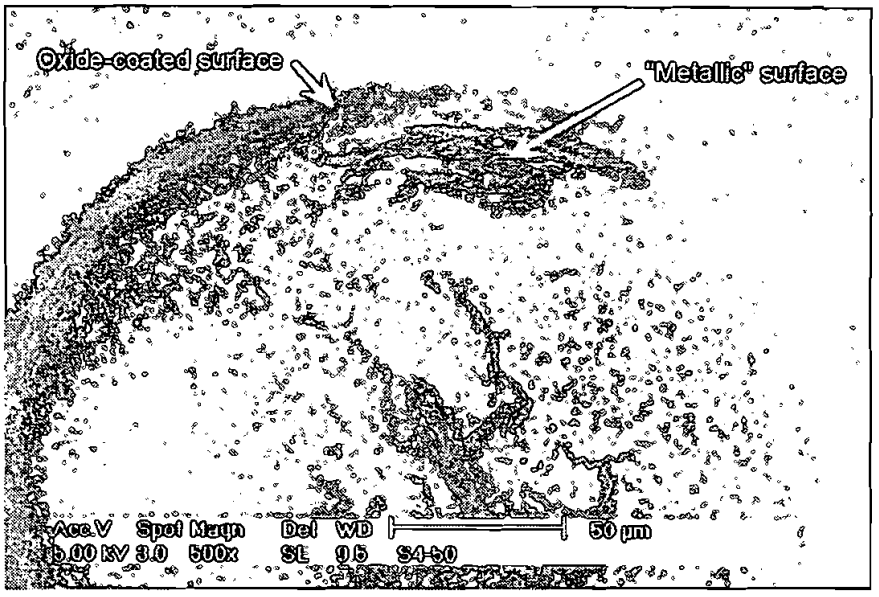

FIGURE 9 Portion of the surface of a quenched aluminum particle without an oxide layer

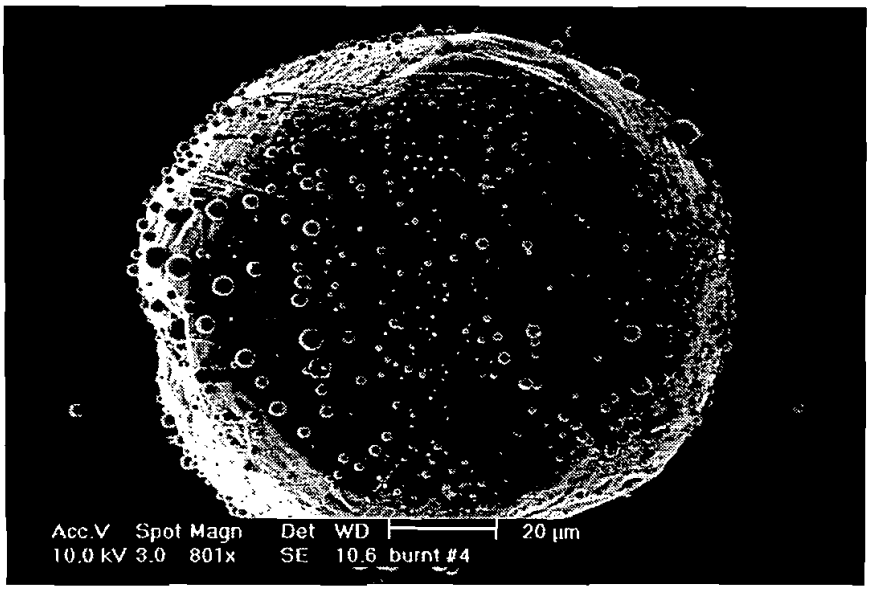

FIGURE 10 Residue of aluminum particle with initial diameter of 250 µm completely burnt in CO_2

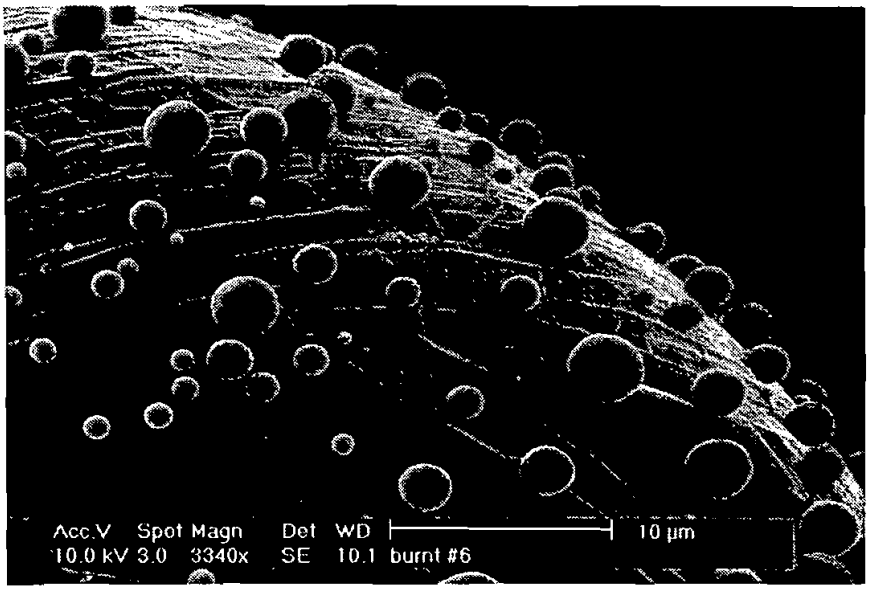

FIGURE 11 Close-up view of the surface of the residue of aluminum particle completely burnt in CO_2

that the cross-sectioned particle surfaces appear clean. Both oxygen and carbon were found inside the particles quenched at different times. The elemental compositions averaged over the entire cross-sections for different quench times are shown in Fig. 12. Carbon is present in higher quantities than oxygen that is consistent with its higher solubility in molten aluminum as compared to oxygen.

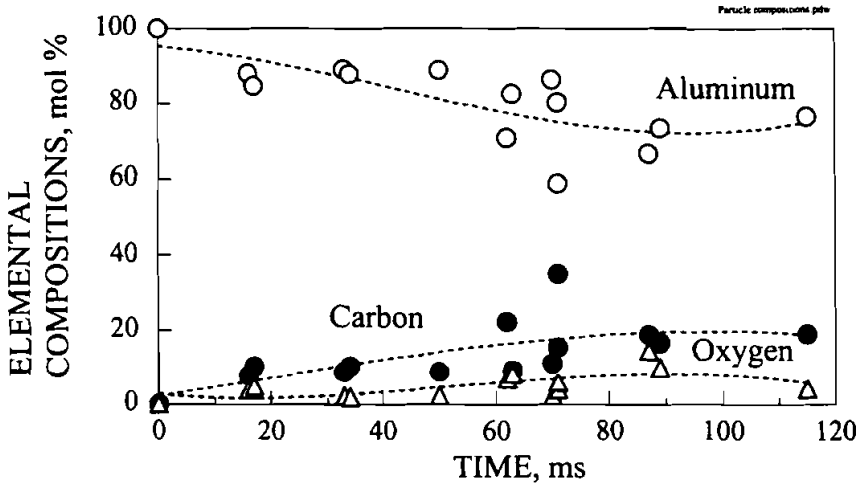

FIGURE 12 Averaged elemental compositions of aluminum particles burning in CO_2 as a function of combustion time

Detailed concentration profiles for Al, C, and O along an arbitrary diameter in a typical rapidly quenched sample are shown in Fig. 13. The small gradients in the elemental compositions observed from Fig. 13, are consistent with the fairly uniform brightness of the back-scattered electron (BSE) images of the particle cross-sections that usually reveal the brightness contrast between phases with different metal contents. An example of a BSE image of a cross-sectioned, rapidly quenched particle is shown in Fig. 14.

For the completely burnt particles, characteristic mixed phase patterns are observed, as shown in Fig. 15, that are typical of the eutectic phase separation (Rhines 1956). Discussed above surface morphology of the burnt particles (Figs. 10, 11) can be associated with this observed from the cross-sections internal layered morphology: different phase layers projected onto the surface would produce visible cracks. It is also interesting that the 1–5 μm diameter oxide spheres observed on the surfaces of the burnt aluminum particles (cf. Figs. 10, 11) are also observed on particle cross-sections (cf. Fig. 15). It indicates that, unlike the oxide layer composed of nano-spheres found on the quenched particles, the 1 – 5

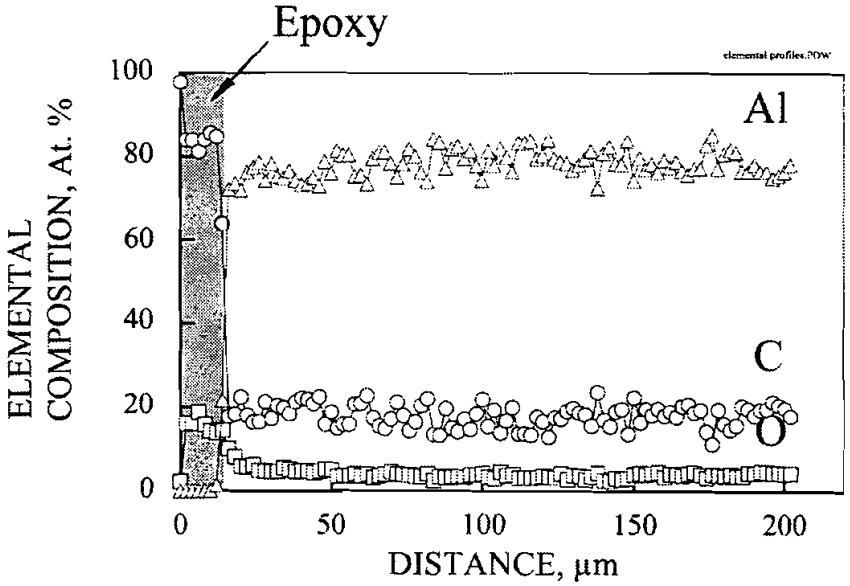

FIGURE 13 Elemental composition profiles across diameter of cross-sectioned aluminum particle rapidly quenched from CO_2

μm oxide spheres are attached to the burnt particle surfaces strongly enough to withstand the stresses occurring during the sample cross-sectioning and polishing.

TABLE IV Ranges of variation of elemental compositions in the different regions of smoke clouds adjacent to the particles quenched from CO_2 on silicon wafers

Quench Time	*Location of the zone in the cloud*	*C, mol%*	*O, mol%*	*Al, mol%*
13	Internal	2.3 – 16.5	55.1 – 64.7	28.4 – 31.6
	Middle	0	66.9 – 67.0	33.0 – 33.1
	External	0	70.7 – 72.5	27.5 – 29.3
42	Internal	12.4 – 15.4	56.0 – 56.9	28.6 – 30.7
74	Internal	0	63.8 – 64.2	35.8 – 36.2
	Middle	0	65.9 – 66.0	34.0 – 34.1
	External	0	69.7 – 69.8	30.2 – 30.3

The BSE images of the burnt particle cross-sections show clear contrast between phases with different average atomic weights, the phases rich in alumi-

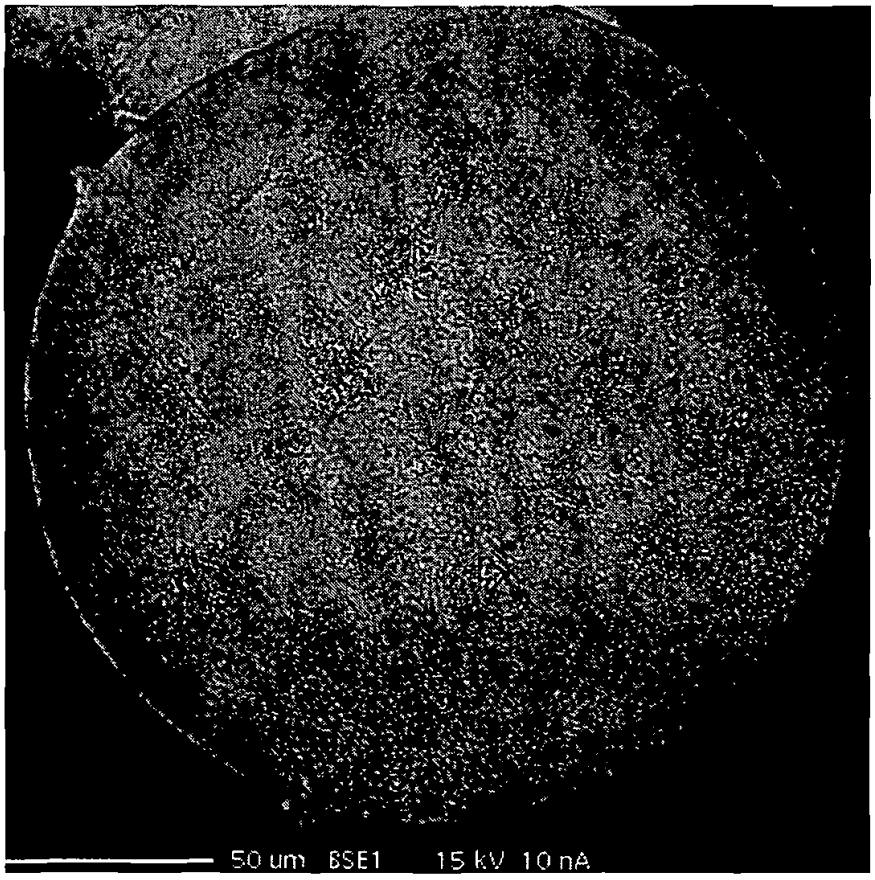

FIGURE 14 Back-scattered electron image of a cross-section of an aluminum particle rapidly quenched from CO_2

num appear lighter, whereas the phases rich in carbon and oxygen appear darker. In addition to the light- and dark-gray layered phases, small white inclusions are visible that are found to be pure aluminum. Several local WDS phase composition measurements were made for each phase that showed the compositions within the phases are indeed uniform, in agreement with the uniform brightness of the phases in the BSE images. Therefore, when different phases could be clearly distinguished, as in Fig. 15, the digitized images were converted using a "Threshold" procedure of the UTHSCSA ImageTool software into three-level gray-scale images so that each gray level represented a phase. The area occupied by each phase was then readily determined using the software and thus, the percentage of each phase in the sample was found. This technique enabled us to ana-

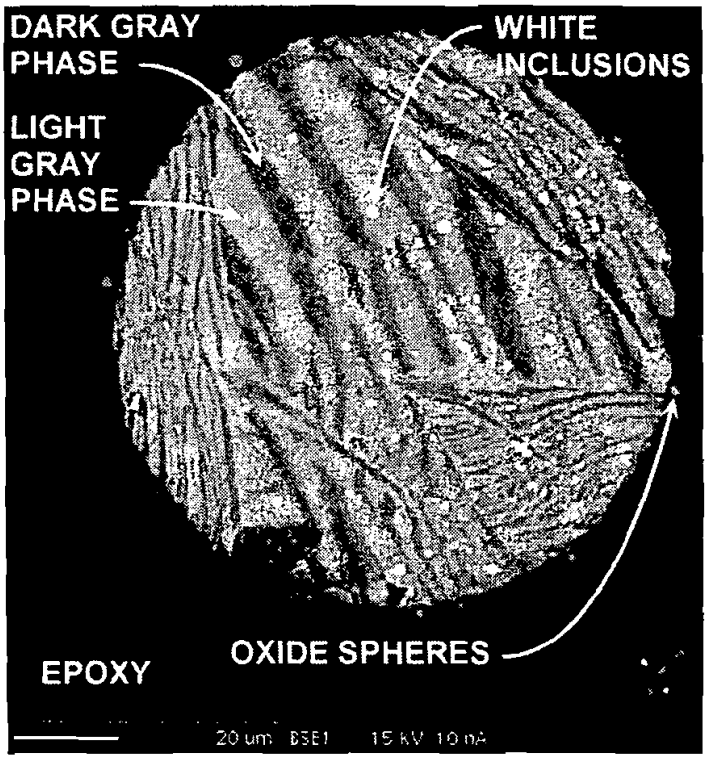

FIGURE 15 Back-scattered electron image of a cross-sectioned aluminum particle burnt in CO_2

lyze a larger number of particles than a more accurate but also a much more time-consuming 2-D WDS elemental mapping of the cross-section surface. An averaged phase composition of the burnt particles is shown in Fig. 16.

FIGURE 16 Averaged phase composition of aluminum particles burnt in CO_2

A comparison of the stoichiometry of the phases found in burnt particles with the aluminum oxy-carbides characterised in the literature that could be matched with those phases is given in Table V. It can be seen that the phases found in the quenched particles contain significantly more aluminum and less oxygen than the known oxycarbides.

TABLE V Aluminum oxycarbides and compositions of phases found in burnt particles

Phase	*Elemental Compositions, mol %*		
	Al	*C*	*O*
Al_4C_3	57	43	0
Al_4O_4C	45	6	49
Al_2OC	50	25	25
White phase	100	0	0
Light Gray Phase	92.2	5.45	2.35
Dark Gray Phase	56.75	35.8	7.45

IV. DISCUSSION

COMBUSTION RATE

Aluminum particles were observed to burn in CO_2 faster than in air. It has also been observed that the d^2-law, which implies that the particle combustion is diffusion limited, is not adequate for the description of the experimental dependency of the aluminum combustion time in CO_2 on the particle size. The classic, diffusion controlled droplet combustion model predicts that the rate of combustion of aluminum in CO_2 is higher than that in air due to the higher oxidizer concentration. Indeed, the evaporation coefficient β entering the d^2-law expression for the size of burning droplet d as a function of time, t: $d^2 = d_0^2 - \beta t$, can be estimated and compared for air and CO_2. According to the Frössling correlation for a particle burning in air in the presence of forced convection (Williams, 1985):

$$\beta = \frac{8\lambda_g}{C_p \rho} \ln(1 + B) \cdot (1 + 0.276\ \mathrm{Re}^{1/2}\ \mathrm{Pr}^{1/3}) \qquad (1)$$

where ρ is the density of liquid metal, λ is the gas thermal conductivity, C_p is the gas heat capacity, B is the transfer number, and Re and Pr are the Reynolds and Prandtl numbers, respectively. The transfer number B is given by (Glassman, 1993):

$$B = \frac{\lfloor Q_{Ox} X_{Ox,\infty} + C_p(T_\infty - T_S) \rfloor}{L} \tag{2}$$

where Q_{Ox} and $X_{Ox,\infty}$ are respectively the energy released in combustion per mole of oxidizer and the mole fraction of the oxidizer present in the external environment, L is the latent heat of vaporization of the droplet, T_∞ is the temperature of the environment, and T_S is the temperature at the surface assumed to be equal to the boiling point of metal.

For aluminum combustion in CO_2 the following reaction needs to be considered:

$$2/3Al + CO_2 \rightarrow 1/3Al_2O_3(l) + CO \text{ with } Q_{CO2} = 495.5\ kJ/mol \tag{3}$$

For aluminum combustion in air, the reaction is:

$$4/3\ Al(g) + O_2 \rightarrow 2/3\ Al_2O_3(l) \text{ with } Q_{O2} = 1556.7\ kJ/mol \tag{4}$$

The transfer numbers for both air and CO_2 estimated using Eq. (2) are:

$$B_{CO2} \approx 1.5; \quad B_{Air} \approx 1.0 \tag{5}$$

The evaporation rate coefficients were estimated using particle velocity of 2 m/s (a typical experimental velocity for a 250 μm particle) for both air and CO_2. The estimated evaporation coefficients for CO_2 and air, respectively, are:

$$\beta^{est}_{CO2} = 2.6 \cdot 10^{-3}\ cm^2/s; \quad \beta^{est}_{Air} = 1.7 \cdot 10^{-3}\ cm^2/s \tag{6}$$

For air, β^{est}_{Air} was compared with the respective parameter of the power function best fit to the experimental combustion times of aluminum particles burning in air. The exponent of the best-fit power function was equal to 1.9 and $\beta^{exp}_{Air} = 2.06 \cdot 10^{-3}\ cm^2/s$. Thus, for the experimental results on aluminum combustion in air the d^2-law appears to work reasonably well, as in the earlier research, e.g., (Price, 1984). A somewhat higher value of the evaporation coefficient for CO_2 indicates the anticipated higher rate of the diffusion-controlled combustion. However, the direct comparison of the estimated β^{est}_{CO2} with the fitting parameters for the experimental results could not be made because the exponent of the curve fitting the experimental points was equal to 2.65, i.e., significantly different from 2. The slope of the $d^2(t)$ dependency steeper than that of the d^2-law implies that a rate process proportional to the particle volume (e.g., ~ d^3) could be important, in addition to the rate process proportional to the particle surface (e.g., diffusion rate ~ d^2). Indeed, as discussed above, the evidence of internal reactions occurring in burning particles has been found from the particle composition analyses, and the experimental $d^2(t)$ dependence indicates that these reactions played a role in determining the overall combustion rate.

ADIABATIC FLAME TEMPERATURES AND REACTION PRODUCTS

Adiabatic flame temperatures and produced species for different equivalence ratio Al-CO_2 flames and, for reference, for Al-air flames, were computed using an AFAL specific impulse code (Selph and Hall, 1991) and initial reagents temperature of 300 K. The database of products was expanded to include the described in the literature (Cox and Pidgeon, 1963; Qiu, and Metselaar, 1995; Qiu and Metselaar, 1997) condensed aluminum oxycarbide phases:

Al_4O_4C: Molar enthalpy $\Delta H^0_{298\ K}$=-543.1 kcal; Entropy $\Delta S^0_{298\ K}$=25 e.u.; and heat capacity C_p=51.42+4.82·10^{-3}T-15.30·10^5T^{-2} kcal/mol/K;

Al_2OC: Molar enthalpy $\Delta H^0_{298\ K}$=-171.5 kcal; Entropy $\Delta S^0_{298\ K}$ =6.5 e.u.; C_p=23.93+2.00·10^{-3}T-6.92·10^5T^{-2} kcal/mol/K;

The results of computations for Al-CO_2 flame are presented in Fig. 17. It is interesting that the adiabatic flame temperature has a very sharp peak at the equivalence ratio $\varphi = 1$ and decreases by about 500°C at $\varphi = 0.7$ and $\varphi = 1.3$. For comparison, the change in the adiabatic flame temperature for Al-air flame at the same range of the equivalence ratios is less than 100 °C. As shown in Fig. 17, at high equivalence ratios in the Al-CO_2 flame, the formation of significant amounts of Al_2OC is predicted that maintains relatively high adiabatic flame temperature of about 2400 °C over a wide range of the fuel/oxidizer ratio variation.

COMBUSTION TEMPERATURES

The measured temperature for aluminum combustion in air of around 2727 °C that is considerably less than the respective adiabatic flame temperature of (3523 °C), is in agreement with the results reported earlier using the same experimental setup (Dreizin 1996; Dreizin, 1999b). In CO_2 the highest measured temperature is around 3000 °C, reasonably close to the estimated adiabatic flame temperature of 2823 °C. In both air and CO_2 the measured temperatures are well above 2467 °C, the boiling point of pure aluminum. Radiation intensity from the stand-off flame in air exceeds, for the most of the combustion time, the radiation from the particle surface and the measured temperature decreases when the intensity of the stand-off flame radiation weakens. These observations indicate that the measured color temperature characterizes vapor-phase flame zone rather than the particle surface. However, it is interesting that the temperature measured in CO_2 remains high even after the vapor phase reaction decays, based on the comparison of the radiation intensities at the AlO and black body spectral bands, as described above. After the radiation intensity of the vapor phase flame decreases,

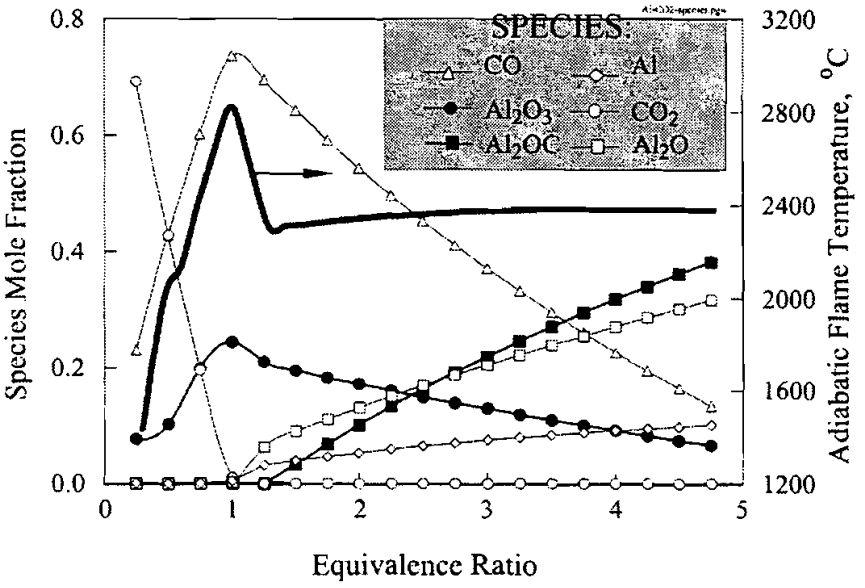

FIGURE 17 Adiabatic flame temperature and main products of the Al-CO_2 flames at different equivalence ratios

most of the signal affecting the input of the color pyrometer was produced by the particle surface. Therefore, it appears that during aluminum combustion in CO_2, the particle surface was at a temperature noticeably higher than the aluminum boiling point. Significant amounts of carbon and oxygen found in the interiors of the quenched particles could increase the boiling point of the produced high-temperature Al-C-O phase as compared to the pure aluminum.

PARTICLE SURFACE LAYER FORMATION

The oxide layer found on particles quenched in CO_2 consisted of the partially coalesced nano-spheres of alumina. The size of the nano-particles is similar to that of the particles in the smoke cloud trace and is typical for the particles produced in the vapor-phase reaction. The smoke cloud trace on the plate forms when the smoke cloud surrounding the burning particle settles down as a result of particle impinging upon the plate. However, the number density of the oxide nano-spheres on quenched particle surface was much greater than that in the smoke cloud immediately at the surface. In addition, carbon traces were detected in the cloud in proximity of the particle surface, but not on the particle surface.

These differences indicate that the mechanism of formation of the oxide coating on the quenched particles is different from that of formation of the smoke cloud trace on the quenching plate. It is suggested that the coating have been produced during the particle combustion due to the transport of the vapor phase combustion products towards the burning particle surface. Thermophoresis could have played an important role in the transporting the products from the vapor-phase combustion zone because of the very sharp temperature gradient expected in the Al-CO_2 flame based on a sharp change of the adiabatic flame temperature at varying equivalence ratio (Fig. 17). In addition, the effect of diffusiophoresis due to aluminum evaporation from the particle surface and production of condensed products in the flame zone, that efficiently counteracts the thermophoresis in the Al-air flame, is reduced because one of the products formed in the vapor-phase Al-CO_2 flame is gas, CO.

When the vapor-phase combustion becomes less active, as indicated by the comparison of the black body and AlO radiation intensities, it is expected that the oxide layer on the particle will be formed less actively, and eventually, will not be formed at all. Accordingly, particles quenched at later combustion times were observed to have parts of their surfaces free of oxide coating, and burnt particles did not have any surface oxide layer.

The large size of the oxide spheres attached to the surface of burnt particles (cf. Fig. 10, 11) indicates that they have not been formed from the gas phase. Their morphology indicates that liquid oxide could be expelled to the surface of the droplet as a result of an internal phase separation, e.g., during solidifying of the droplet or a part of the droplet at a temperature exceeding the Al_2O_3 melting point.

INTERNAL PHASE CHANGES

The experimental combustion temperatures for aluminum burning in carbon dioxide are high and therefore, high-temperature phases and phase changes need to be considered in order to understand and model combustion. The complex Al-O-C phases found in the quenched particles further support the need of inclusion of the internal phase modifications and changes in the combustion mechanism. Unfortunately, the ternary Al/C/O phase diagram could not be found in the literature and binary Al/C and Al/O phase diagrams (Massalski, et al., 1990; Levinskiy, 1990) were used together with the pseudo-binary phase diagram of Al_2O_3/Al_4C_3 (Qui and Metselaar, 1997) to qualitatively analyze the phases and phase changes expected to occur during combustion. The described in the literature oxycarbide phases include Al_2OC, Al_4O_4C, and a number of saturated liquid Al-C-O solutions found in the Al_2O_3/Al_4C_3 phase diagram. However, the com-

positions of the quenched and burnt particles (e.g., Figs. 12, 13, 16) do not match any of these compounds produced generally at very high carbon and oxygen contents (e.g., using Al_2O_3 and Al_4C_3 as precursors). Therefore, a research focused at the high-temperature, aluminum-rich portion of the ternary Al/O/C system is necessary to accurately interpret the experimental observations made in this research. The following discussion presents only a very crude attempt to correlate the phase changes occurring with the phases described in the literature with the observations on aluminum combustion in CO_2. Table VI summarizes information on various phase equilibria in all three binary systems considered (Al/O, Al/C, and Al_2O_3/Al_4C_3) at high temperatures. Phases denoted as Al-O (l), Al-C (l), and Al-C-O (l) indicate liquid solutions. For the Al/O system, (l_1) and (l_2) denote oxygen-rich and oxygen-lean liquid solutions, respectively. Each horizontal line in the table indicates a phase change. The phases that can exist in equilibrium before and after the phase change can be found above and below each line, respectively. The phase diagrams imply that a variety of liquid phases can be produced in the Al/O/C system at the temperatures exceeding 2467 °C, the pure aluminum boiling point. It is, therefore, appears reasonable to expect that after ignition pure molten aluminum interacting with carbon and oxygen-containing species forms a liquid Al-O-C solution. The formation of such a solution can occur through surface reactions of molten aluminum with CO, CO_2 and, possibly, oxycarbide and suboxide species produced in the vapor-phase flame. Specifically, exothermic surface reaction of molten aluminum and CO has been observed by Bucher et al., 1999, however, detailed experimental data are not available.

As Table VI shows, equilibrium gas phases disappear for the Al/O system at temperatures below 2237 °C. Thus, gas-phase reactions are expected to cease below this temperature. However, it is also indicated in Table VI that for the carbon-containing species, equilibrium gas phases stop being produced at noticeably higher temperatures. Therefore, it is expected that the rate of the aluminum droplet gasification decreases dramatically when its carbon content increases. Such a change in the gasification rate could explain a rapid decrease in the intensity of the vapor-phase reaction observed experimentally (cf. Fig. 3).

At a very narrow temperature range, 2160 – 2173 °C, non-variant phase transitions occur in both Al/C and Al_2O_3/Al_4C_3systems. A non-variant phase transition in the Al/C system at 2173 °C produces a saturated liquid Al-C solution with about 19 atomic % of carbon, solid aluminum carbide, and graphite. At 2160 °C, a non-variant phase change occurs in the Al_2O_3/Al_4C_3 system producing a saturated liquid Al-O-C solution (~ 65 % of Al_4C_3) and graphite. It is, therefore, suggested that when the burning particle temperature decreases to this temperature range (2160–2173 °C) a phase change resulting in the formation of at least one

solid phase occurs. At a lower temperature of 2050 °C, solidification of alumina occurs that causes phase changes in both Al/O and Al_2O_3/Al_4C_3 systems producing the solid Al_2O_3 phase. It is, therefore, likely that alumina will also be produced at this temperature in the cooling burnt particles. The observed phase composition and morphology of the burnt particles can be related to this expected sequence of phase changes occurring during their cooling. Micro-spheres of alumina were observed on surface of the burnt particles and pure aluminum inclusions were found inside the particles. Thus, it appears reasonable to suggest that a phase transition occurs upon particle cooling to approximately 2160 °C resulting in the production of at least one solid and one liquid Al-O-C phases and liquid alumina. The expelling of alumina onto the particle surface could occur due to immiscibility of the precursor phases. Liquid alumina indeed is known to be immiscible with the molten aluminum and aluminum-rich Al-O solutions (Massalski, et al., 1990) that are expected to have properties similar to the currently uncharacterized aluminum-rich oxycarbide phases found in the burnt particles. The spherical shape and large size of the alumina particles implies that alumina was liquid when it appeared on the burnt particle surface and it was produced as a result of a condensed phase separation rather than a vapor-phase reaction. An additional argument supporting the mechanism of alumina formation as a result of phase separation occurring in the particle comes from the observation of strong attachment of large alumina spheres to the particle surface in contrast with the very weak bonding between the nano-particle oxide layer and surface of the particles quenched during their combustion. Thus, when particle continues to cool to 2050 °C, alumina solidifies. The ternary liquid Al-C-O solution (aluminum-rich and oxygen-lean) that is expected to exist in the particles at the temperatures below 2050 °C can be compared to the aluminum-rich Al/C solution described in the Al/C phase diagram (Massalski, et al., 1990). Such a solution remains uniform until approximately 660 °C (aluminum melting point, not included in Table VI), however, the carbon solubility limit decreases at lower temperatures and drops dramatically at temperatures below 1500 °C. The continuous decrease in the carbon solubility limit during the particle cooling could result in the formation of small islands of pure aluminum observed inside burnt particles. Note again that the above discussion is not supported by an accurate Al/O/C phase diagram and additional information about the high-temperature, aluminum-rich phases formed in the Al/O/C system and their mutual miscibility is necessary to understand the morphology of the quenched and burnt particles. Energetics of different oxycarbide phases must be known to understand the mechanism of the heat release causing the observed in CO_2 spear-points.

TABLE VI High-Temperature Phases in binary systems containing Al, C, and O

Temperature °C	*Phases Existing in a System*		
	Al/O	*Al/C*	*Al_2O_3/Al_4C_3*
> 4827	Gas	Gas	Gas
3550 – 4827		Gas + Al-C (l) + C	
2980 – 2467	Gas + Al-O (l_1)		Al-O-C (l)
2467 – 2237	Gas + Al-O (l_1) + Al-O (l_2)	Al-C (l) + C	Al-O-C (l) + C
2237 – 2173	Al-O(l_1) + Al-O (l_2)		
2173 – 2160		Al-C(l) + Al_4C_3 + C	
2160 – 2050			Al-O-C (l) + Al_4C_3
2050 – 1990	Al-O (l_2) + Al_2O_3		Al-O-C (l) + Al_4C_3 + Al_2O_3
1990 – 1870			Al-O-C (l) + Al_2OC+ Al_4C_3 + Al_2O_3
1870 – 1850			Al-O-C (l) + Al_2OC+ Al_4C_3 + Al_4O_4C + Al_2O_3

CONCLUSIONS

Combustion of aluminum particles free-falling in CO_2 has been studied experimentally and combustion times and temperatures were measured for a range of particle sizes. Preliminary experiments with particles of commercially available aluminum-rich Al-Mg and Al-Si alloys were also performed. The size of the burning particles was observed to decrease and, based on the particle size measurements, it was found that more than 94 % of aluminum was consumed by combustion in CO_2. It was found that the rate of aluminum combustion in CO_2 is faster than that in air and the dependence of particle burn time from particle size is best described by $t \sim d^{2.5}$ rather than by $t \sim d^2$-law. Flame radiation measurements showed that the vapor-phase reaction is significant only during the initial period of combustion. The temperature measured using a three-color pyrometer was steady and around 3000 °C during most of the combustion time. The estimated adiabatic flame temperature is reasonably close to the experimental value. Particles quenched on Si wafers were surrounded by spherical smoke clouds and the particle surfaces were coated with a layer of partially coalesced oxide nano-spheres. The morphology and sizes of the nano-spheres on particle surface were the same as for the oxide nano-particles in the cloud. However, the smoke cloud particles contained traces of carbon whereas no carbon was detected in the particle coating. Also, the number density of oxide nano-spheres in particle coating was much greater than that in the cloud trace immediately adjacent to the par-

ticle surface, indicating that the particle surface oxide coating was formed during combustion rather than due to settling of the smoke on the quenched particle. Surfaces of the completely burnt particles did not have a continuous oxide coating. Instead, a number of oxide spheres in the size range of 1 – 5 μm were attached to the particle surface. Interiors of the particles rapidly quenched on aluminum foil were uniform and contained significant amounts of carbon and oxygen. Some increase in the overall carbon and oxygen content was observed at longer combustion times. Interiors of the completely burnt particles contained several mixed phases, including layers of two non-stoichiometric aluminum oxycarbides and pure aluminum inclusions. None of the oxycarbide phases detected in the quenched or burnt particles was similar to the aluminum oxycarbides described in literature. Analyses of the experimental results have indicated possible importance of the thermophoretic flows in the transport of the vapor-phase reaction products. It has also been suggested that the internal phase changes affect significantly the temperature and rate of aluminum combustion in CO_2. This research presents the first attempt of the systematic experimental characterization of aluminum combustion in CO_2 and it appears that additional experiments are needed to develop a complete combustion model.

Acknowledgements

This work has been partially supported by The National Center for Microgravity Research on Fluids and Combustion. The authors appreciate the help in the organization of experiments and support from the research staff of AeroChem Research Laboratory, Titan Corporation. The authors also would like to acknowledge assistance of Dr. E.P. Vicenzi (currently with Smithsonian Institution) in sample characterization using electron microscopy.

References

Bucher, P., Yetter, R.A., Dryer, F.L., Vicenzi, E.P., Parr, T.P., and Hadson-Parr, D.M., "Condensed Phase Species Distribution about Al Particles Reacting in Various Oxidizers" *Combust. Flame* 117:351–361 (1999).

Cox, J. H., and Pidgeon, L. M., "An Investigation of the Aluminum-Oxygen-Carbon System," *Can. J. Chem.*, 41, pp. 671–683, 1963.

Dreizin, E.L., Suslov, A.V., and Trunov, M.A., "General Trends in Metal Particle Heterogeneous Combustion,", *Combust Sci. Techn.*, *89*, 22 (1993).

Dreizin, E.L., "Experimental Study of Stages in Aluminum Particle Combustion in Air", *Combust. Flame*, 105:541–556 (1996).

Dreizin, E.L., "Experimental Study of Aluminum Particle Flame Evolution in Normal and Micro-gravity", *Combust. Flame*, 116:323–333 (1999a).

Dreizin, E.L., "On the Mechanism of Asymmetric Aluminum Particle Combustion", *Combust. Flame* 117:841–850 (1999b).

Glassman, I, "Combustion" Acad. Press, New York, San Francisco, London (1993).

Legrand, B., Shafirovich, E., Marion, M., Chauveau, C., and Gökalp I., "Ignition and Combustion of Levitated Magnesium Particles in Carbon Dioxide" Twenty-Seventh Symposium (Int'l) on Combustion (1998).

Legrand, B., Marion, M., Chauveau, C., Gökalp I., and Shafirovich, E., "Ignition and Combustion of Levitated Magnesium and Aluminum Particles in Carbon Dioxide" 17th International Colloquium on the Dynamics of Explosions and Reactive Systems, Heidelberg, Germany, July 1999.

Levinskiy, Y.V., "P-T-X Binary Phase Diagrams of Metal Systems", Moscow, Metallurgia, (1990) (In Russian).

Massalski, T.B., Okamoto, H., Subramanian, P.R., and Kacprzak, L. (Eds) "Binary Alloy Phase Diagrams", ASM Publ., Materials Park, OH, 1990.

Marion, M., Gonthier, F., Chauveau, C., and Gökalp, I., "Studies on the Burning of Levitated Aluminum Particles: Effects of Variable CO_2 Concentration under Pressure" *Chemical and Physical Processes in Combustion*. The Eastern States Section of The Combustion Institute, December 1996, Hilton Head, SC, pp. 483–486.

Marion, M., Legrand, B., Chauveau, C., and Gökalp, I., "Studies on the Burning of Levitated Aluminum Particles: Effects of CO_2 and Pressure" *33rd AIAA/ASME/SAE/ASEE Joint Propulsion Conference and Exhibit*, July 6–9, 1997, Seattle, WA.

Molodetsky I.E., Dreizin, E.L., Law C.K., "Evolution of Particle Temperature and Internal Composition for Zirconium Burning in Air" *Twenty-Sixth Symposium (Int'l) on Combustion*, The Combustion Institute, Pittsburgh, 1997, pp. 1919–1927.

Molodetsky, I.E., Dreizin, E.L., Vicenzi, E.P., Law, C.K., "Phases of Titanium Combustion in Air" *Combust. Flame*, 112:522–532 (1998).

Nelson, L. S., *Eleventh Symposium (Int'l) on Combustion*, The Combustion Institute, Pittsburgh, 1967, pp. 409–416.

Pearse, R.W.B., and Gaydon, A.G., "The identification of molecular spectra". Halsted Press, NY, 1976.

Prentice, J.L., (Ed.), "Combustion of pulse heated Single particles of Aluminum and Beryllium", NWC TP5162, Naval Weapons Center, China Lake, CA, 1971.

Price, E.W., in "Fundamentals of Solid Propellant Combustion" (K.K. Kuo and M. Summerfield, Eds.), AIAA, New York, 1984, pp. 479–514.

Qiu, C., and Metselaar, R., "Thermodynamics Evaluation of the Al2O3-Al4C3 System and Stability of Al-oxycarbides," Z. *Metallkd.*, 86 [3], pp. 198–205, 1995.

Qiu, C., and Metselaar, R., "Phase Relations in the Aluminum-Carbide-Aluminum-Nitride-Aluminum-Oxide System," *J. Am. Ceram. Soc.*, 80 [8], pp. 2013–2020, 1997.

Rhines, F.N., "Phase Diagrams in Metallurgy, Their Development and Application", McGrow Hill, New York, Toronto, London (1956).

Rieder, R., Economou, T., Wänke, H., Turkevich, A., Crisp, J., Brückner, J., Dreibus, G., and McSween, H.Y. "The Chemical Composition of Martian Soil and Rocks Returned by the Mobile Alpha Proton X-ray Spectrometer: Preliminary Results from X-ray Mode" *Science* 278: 1771–1774 (1997).

Shafirovich, E.Y., and Goldshleger, U.I., "The Superheat Phenomenon in the Combustion of Magnesium Particles" *Combustion and Flame* 88:425–432 (1992).

Shafirovich, E.Y., and Goldshleger, U.I., "Combustion of Magnesium Particles in Carbon Dioxide and Monoxide" *J. Propulsion Power* 13:395–397 (1997).

Selph, C., and Hall, R., "AFAL Specific Impulse Program" Phillips Labs, Propulsion Directorate, RKCC, Edwards AFB, CA (1991) (updated periodically).

Suslov, A.V., Dreizin, E.L., and Trunov, M.A. "Formation of Monodisperse Refractory Metal Particles by an Impulse Discharge", *Powder Techn. 74*, 23 (1993).

Valov, A.E., Kustov, Y.A., and Shevtsov, V.I., "Spectroscopic Study of the Combustion of Solitary Magnesium Particles in Air and in Carbon Dioxide" *Combustion, Explosion, and Shock Waves* 30:431–436 (1994).

Williams, F. A., "Combustion Theory". Benjamin/Cummings Publishing Co., Menlo Park California, 1985.

Wilson R. P. Jr., Williams F. A., "Experimental Study of the Combustion of Single Aluminum Particle in O_2/Ar", *Thirteenth Symposium International on Combustion*, The Combustion Institute, Pittsburgh, PA, pp. 833–845 (1971).